International Journal of Solids and Structures 49 (2012) 959–972

Contents lists available at SciVerse ScienceDirect

International Journal of Solids and Structures

journal homepage: www.elsevier.com/locate/ijsolstr

The Brazilian disc under parabolically varying load: Theoretical and experimental study of the displacement field

S.K. Kourkoulis *, Ch.F. Markides, P.E. Chatzistergos

National Technical University of Athens, School of Applied Mathematical and Physical Sciences, Department of Mechanics, Laboratory for Testing and Materials, 5 Heroes of Polytechnion Avenue, Theocaris Bld., Zografou Campus, 157 73 Athens, Greece

ARTICLE INFO

Article history:
Received 29 September 2011
Received in revised form 24 November 2011
Available online 20 January 2012

Keywords:
Brazilian disc test
Contact problems
Complex potentials
PMMA
Marble
Digital image correlation (DIC)

ABSTRACT

The displacement field in an intact Brazilian disc under the influence of a parabolically varying radial pressure distribution acting along two symmetric arcs of its periphery is studied. The specific loading type closely approaches the actual load-distribution as obtained by considering the specimen and the load platen as a system of two elastic bodies in contact. The problem is solved adopting the complex potentials method and a closed form full-field solution is proposed. The results of the theoretical analysis for discs made either from Dionysos marble or PMMA are considered in juxtaposition to the respective ones obtained for uniform radial pressure as well as for concentrated point load. Critical points related to the variation of the displacement field in the immediate vicinity of the load platen-specimen interface are enlightened. The accuracy of the solution is assessed by comparing the analytic results with the experimental ones obtained from series of Brazilian-disc tests carried out using the standardized device suggested by the international society for rock mechanics. The specimens were made from PMMA and the 3D digital image correlation technique was employed for measuring the components of the displacement field developed. It is proved that the experimental results are in very good qualitative and quantitative agreement with the theoretical predictions.

1. Introduction

The most popular substitute of the direct tension test, especially for specimens made from brittle geomaterials, is perhaps the Brazilian-disc test, i.e. the diametral compression of short cylinders. The test was introduced independently and almost simultaneously (Machida, 1975; Fairbairn and Ulm, 2002) by Carneiro (1943) and Akazawa (1943).

Two approaches are widely adopted nowadays for the standardized laboratory execution of the test, i.e. the one suggested by the international society for rock mechanics (ISRM, 1988) and that suggested by the American society for testing and materials (ASTM, 1988). In the first one the disc is squeezed between curved metallic jaws, of predefined curvature, representing a curve-to-curve contact problem while in the latter the disc is compressed between plane jaws corresponding to a curve-to-plane contact problem.

From the theoretical point of view the vast majority of studies about the Brazilian-disc test do not take into consideration the interaction between the loading platens and the specimen. In most cases the disc is considered either under compressive point forces across a diameter (Muskhelishvili, 1963; Colback, 1967; Claesson and Bohloli, 2002; Tong et al., 2007; Jianhong et al., 2009) or under uniform pressure (radial or not) acting along two symmetric arcs of arbitrarily predefined "small" length (Hondros, 1959; Fairhurst, 1964; Vardar and Finnie, 1975; Markides et al., 2010). It is exactly the adoption of these two assumptions (point- or uniform-load and constant length of the loaded arc) that jeopardizes the validity of these approaches, although they are widely applied for practical purposes with more or less satisfactory results. This is due to the fact that the stress field at the center of the disc is more or less insensitive to the exact variation of the external load applied along the contact arc (Lavrov and Vervoort, 2002; Markides et al., 2011). Obviously this is not the case in the immediate vicinity of the load application area. Here the local stress field strongly depends not only on the magnitude of the contact length but, also, on the exact distribution of the radial pressure and perhaps friction, inevitably appearing in case the specimen's and jaw's materials have different elastic properties (Hooper, 1971; Wijk, 1978).

In this context an attempt is described here to cure (at least partly) the above weaknesses by taking into account the "actual" distribution of radial pressure exerted on the disc by the metallic jaw (loading platen) as it is obtained when the disc and the jaw are considered as a system of two mutually interacting elastic bodies in contact. Attention is focused to the test standardized by ISRM which is based on the apparatus, shown in Fig. 1. The

* Corresponding author. Tel: +30 210 7721263; fax: +30 210 7721302.
E-mail address: stakkour@central.ntua.gr (S.K. Kourkoulis).

0020-7683/$ - see front matter © 2012 Elsevier Ltd. All rights reserved.
doi:10.1016/j.ijsolstr.2011.12.013

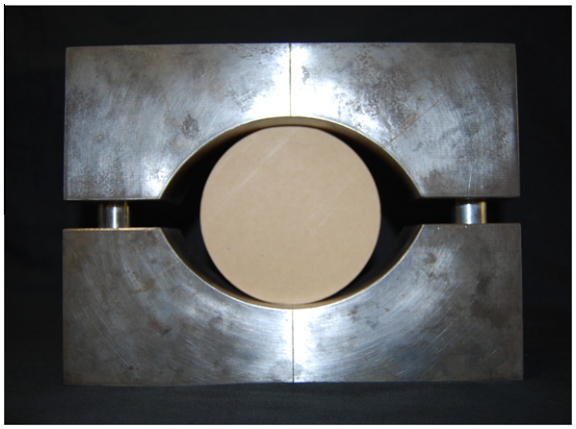

Fig. 1. Photo of the ISRM suggested device for the standardized realization of the Brazilian-disc test, for discs with R = 50 mm.

apparatus consists of two identical metallic jaws of curvature radius R_{jaw} equal to 1.5R (R is the disc-shaped specimen' radius). It is evident that in case the own weight of the jaws is ignored the contact is initially realized along a mathematical line, i.e. the common generatrix of the two cylindrical surfaces. However, due to the inevitable deformability of the jaw's (which cannot be ignored especially for specimens with elastic modulus comparable to that of the jaws) and disc's materials, as the external load exerted by the loading frame increases the contact is realized along a curved surface the projection of which on the disc's cross section corresponds to the contact arc (symmetric with respect to the vertical axis of symmetry of the arrangement).

The present study is carried out taking advantage of a recent paper (Kourkoulis et al., 2012) which provided an analytic solution for the exact variation of the radial pressure along the contact arc in terms of the disc's and jaw's radii, the elastic properties of the specimen's and jaw's materials and the external load. Clearly the configuration of a Brazilian disc under the above determined type of radial pressure, acting along two predefined arcs of its periphery, corresponds to a first fundamental problem of elasticity which is here solved using the complex potentials method (Muskhelishvili, 1963) and assuming that the contact between the disc and the jaw is smooth (i.e. ignoring any influence of friction stresses). The solution of this problem provides the displacement field in closed form for any point of the disc's surface.

The solution obtained is considered in juxtaposition to the familiar ones for diametral point-load and uniform distribution of radial pressure, assuming static equivalence between the overall loads. It is concluded that at the disc's center the displacement field is indeed completely insensitive to the exact load application mode. On the contrary as the loaded rim is approached the situation changes dramatically, the solutions deviate from each other and erroneous conclusions are drawn in case the actual loading type is not taken into account.

The theoretically obtained field of displacements is compared with the respective one obtained from a series of experiments realized using the ISRM standardized device and the digital image correlation (DIC) technique, which provides the displacements all over the tested disc. Once the displacements are determined one can calculate the strain field and then (assuming linear elasticity) the components of the stress field. The specimens used in the experimental protocol were made from Poly-Methyl-Meth-Acrylate (PMMA) since its mechanical behaviour closely resembles that of a linear elastic material. It is proved that the theoretical results are in very good agreement (both qualitative and quantitative) with the experimentally obtained ones both for displacements and strains. The same is true for the extent of the contact rim, although it is to be mentioned here that a convenient standardized technique for the experimental measure of this quantity is not yet available.

2. Theoretical preliminaries

2.1. The load distribution and the contact length

Consider a system composed of two linearly elastic bodies i.e. the disc shaped specimen and the metallic jaws of the apparatus proposed by ISRM (Fig. 1). Under the assumption of smooth contact between disc and jaw the above configuration corresponds to a plane mixed fundamental problem of classic linear elasticity. In this context, employing Muskhelishvili's complex potentials method for the familiar Hertz problem, Kourkoulis et al. (2012) obtained the radial pressure distribution, P(τ), exerted by the jaw to the disc as (Fig. 2a):

$$P(\tau)=\frac{1}{3RK}\sqrt{\ell^2-\tau^2},\quad K=\frac{\kappa_1+1}{4\mu_1}+\frac{\kappa_2+1}{4\mu_2} \tag{1a}$$

In Eq. (1a) indices 1 and 2 stand for the disc and the jaw, respectively. R represents the disc's radius while κ_1, κ_2 and μ_1, μ_2 are the Muskhelishvili's constants and the shear moduli of the disc's and jaw's materials, respectively. The actual contact angle, ω_o, (or equivalently the actual contact length, l,) was found equal to:

$$\omega_o=\sqrt{\frac{6KP_o}{\pi R}},\quad 2\ell=2\sqrt{\frac{6RKP_o}{\pi}} \tag{1b}$$

P_o is the load exerted by the loading frame, P_{dev}, normalized over the disc's thickness, w.

As it is seen from Eq. (1a) the interaction between jaw and disc represents a radial pressure distribution corresponding to a circular arc (Fig. 2a). Its extent depends on the specimen's radius, the external load and the elastic properties of the disc and jaw's materials.

Given the variation of the radial pressure and the extent of the arcs along which it acts one could proceed to the determination of the displacement field in the disc. However, it is seen that for the specific distribution of P(τ) given by Eq. (1a) a closed form solution can not be obtained. Therefore an alternative distribution, very closely resembling that of Eq. (1a), is introduced here (Fig. 2b) as:

$$P(\tau)=\frac{\pi\ell}{8RK}\left[1-\left(\frac{\tau}{\ell}\right)^2\right] \tag{2}$$

The distribution of Eq. (2) is statically equivalent to that of Eq. (1a) since:

$$\int_{-\ell}^{+\ell}\frac{\pi\ell}{8RK}\left[1-\left(\frac{\tau}{\ell}\right)^2\right]d\tau=\int_{-\ell}^{+\ell}\frac{1}{3RK}\sqrt{\ell^2-\tau^2}d\tau=P_o$$

Introducing now a Cartesian reference system at the center of the disc (Fig. 2b) the following geometrical simplifications (for small values of ω_o) can be adopted:

$$\ell\approx\ell'=R\sin\omega_o,\quad \tau\approx\tau'=R\cos\vartheta,\quad \omega_o=Arc\sin\sqrt{\frac{6KP_o}{\pi R}} \tag{3a}$$

Then in the new coordinates system the pressure distribution of Eq. (2) can be rewritten as:

$$P(\vartheta)=P_c\left(1-\frac{\cos^2\vartheta}{\sin^2\omega_o}\right),\quad P_c=\sqrt{\frac{3\pi P_o}{32KR}} \tag{3b}$$

A circular disc (Fig. 3a) loaded by the radial pressure given by Eq. (3b) along two finite arcs of its periphery (symmetric with respect to its center) represents a first fundamental problem of classic

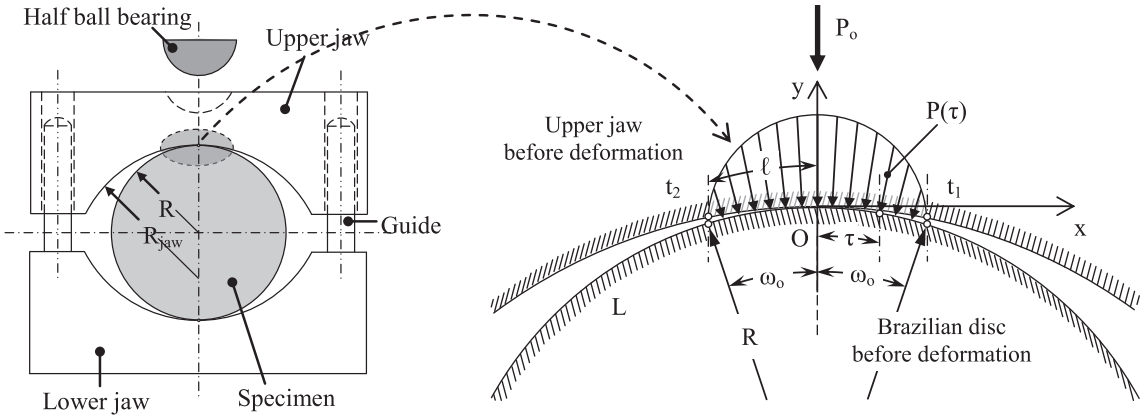

(a)

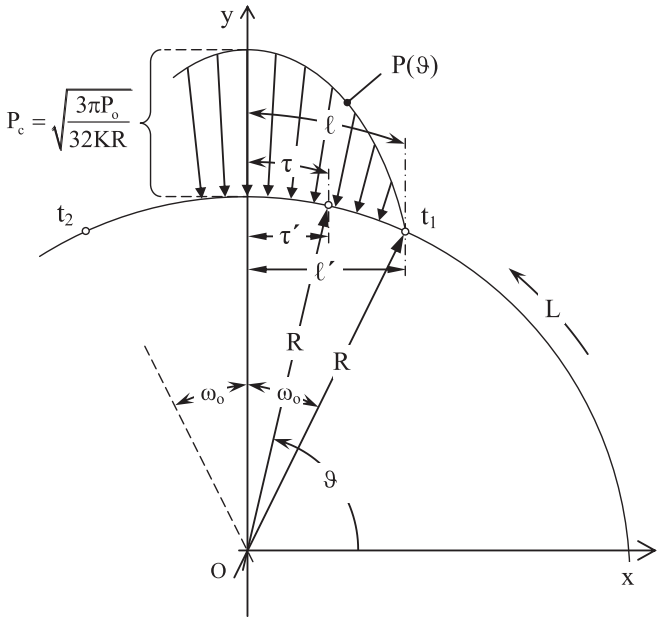

(b)

Fig. 2. (a) The contact problem: definition of symbols and the actual (cyclic) distribution of the radial pressure imposed by the jaw on the disc along the actual contact length $(-\ell, +\ell)$. (b) The Brazilian disc under the parabolic radial pressure distribution considered in the present study.

elasticity. The boundary conditions for the stresses on the disc periphery L read as:

$$\sigma_{rr}^{+}(\vartheta) = -P(\vartheta) = -P_c\left(1 - \frac{\cos^2\vartheta}{\sin^2\omega_o}\right) \text{ on the loaded rims of L,} \quad (4a)$$

$$\sigma_{rr}^{+}(\vartheta) = 0 \quad \text{on the unloaded part of L} \quad (4b)$$

Sign (+) indicates boundary values taken on L from the interior of the disc.

2.2. The complex potentials

Following Muskhelishvili's (1963) technique, based on the complex potentials method, the disc is considered lying in the complex plane$z = re^{i\vartheta}$ (Fig. 3a). Points z on the disc's periphery L are denoted as $t = Re^{i\vartheta}$. The end points of the loaded rims are denoted as t_j $j = 1$, 2, 3, 4. The problem is first solved for the unit disc in the complex plane $\zeta = \rho e^{i\vartheta}$, Fig. 3(b). Points t_j of L through the conformal mapping $z = R\zeta$ correspond to points s_j on the unit circle γ, with $s = e^{i\vartheta}$ the arbitrary point ζ on it. Eq. (4) are now rewritten for γ as:

$$\sigma_{\rho\rho}^{+}(\vartheta) = -P(\vartheta) = -P_c\left(1 - \frac{\cos^2\vartheta}{\sin^2\omega_o}\right) \text{ on the loaded rims of } \gamma, \quad (5a)$$

$$\sigma_{\rho\rho}^{+}(\vartheta) = 0 \quad \text{on the unloaded part of } \gamma \quad (5b)$$

The complex potentials for the problem of the unit disc are written as (Markides et al., 2010):

$$\Phi(\zeta) = \frac{1}{2\pi i}\int_{\gamma}\frac{\sigma_{\rho\rho}^{+}(s)}{s-\zeta}ds - \frac{1}{4\pi}\int_{0}^{2\pi}\sigma_{\rho\rho}^{+}(\vartheta)d\vartheta \quad (6)$$

$$\Psi(\zeta) = \frac{1}{\zeta^2}\Phi(\zeta) + \frac{1}{\zeta^2}\overline{\Phi}\left(\frac{1}{\zeta}\right) - \frac{1}{\zeta}\Phi'(\zeta) \quad (7)$$

Taking now into account that $\cos\vartheta = (s + \bar{s})/2$ Eq. (5a) becomes:

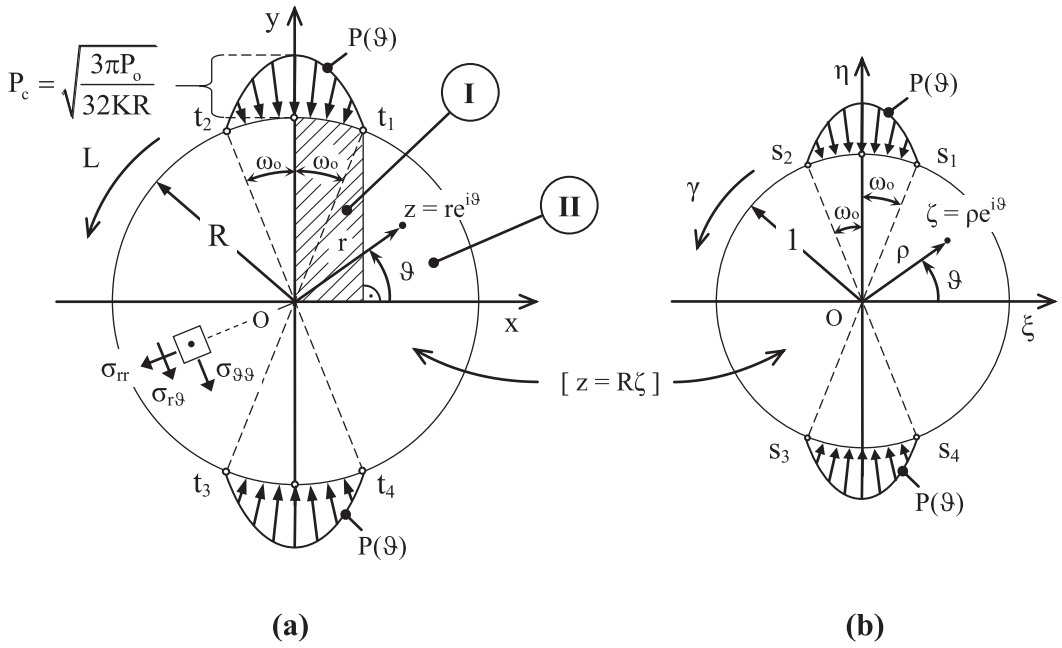

Fig. 3. The conformal mapping.

$$\sigma^{+}_{\rho\rho}(s) = -P_c\left[1 - \frac{1}{4\sin^2\omega_o}\left(2 + s^2 + \frac{1}{s^2}\right)\right] \tag{8}$$

Combination of Eqs. (5) and (8) with Eq. (6) provides (after some lengthy algebra) $\Phi(\zeta)$ as:

$$\Phi(\zeta) = \frac{P_c}{4\pi i\sin^2\omega_o}\left[\left(\frac{\zeta^4+1}{2\zeta^2} + \cos 2\omega_o\right)\ell n\frac{s_2^2-\zeta^2}{s_1^2-\zeta^2} - \left(\frac{1}{\zeta^2} + \cos 2\omega_o\right)2i\omega_o\right] \tag{9}$$

Introducing $\Phi(\zeta)$ from Eq. (9) in Eq. (7) gives for $\Psi(z)$:

$$\Psi(\zeta) = \frac{-P_c}{4\pi i\sin^2\omega_o}\left[\frac{\zeta^4-1}{\zeta^4}\ell n\frac{s_2^2-\zeta^2}{s_1^2-\zeta^2} + \left(\frac{\zeta^4+1}{\zeta^2} + 2\cos 2\omega_o\right)\left(\frac{1}{s_1^2-\zeta^2} - \frac{1}{s_2^2-\zeta^2}\right) + \frac{4i\omega_o}{\zeta^4}\right] \tag{10}$$

For the real disc the complex potentials are obtained through the conformal transformations $\zeta = z/R$, $s_j = t_j/R$ as:

$$\Phi(z) = \frac{P_c}{4\pi i\sin^2\omega_o}\left[\left(\frac{z^4+R^4}{2R^2z^2} + \cos 2\omega_o\right)\ell n\frac{t_2^2-z^2}{t_1^2-z^2} - \left(\frac{R^2}{z^2} + \cos 2\omega_o\right)2i\omega_o\right] \tag{11}$$

$$\Psi(z) = \frac{-P_c}{4\pi i\sin^2\omega_o}\left[\frac{z^4-R^4}{z^4}\ell n\frac{t_2^2-z^2}{t_1^2-z^2} + \left(\frac{z^4+R^4}{z^2} + 2R^2\cos 2\omega_o\right) \times \left(\frac{1}{t_1^2-z^2} - \frac{1}{t_2^2-z^2}\right) + \frac{4iR^4\omega_o}{z^4}\right] \tag{12}$$

3. The displacement field

Integrating the expressions of Eqs. (11) and (12) for $\Phi(z)$ and $\Psi(z)$ the following formulae for $\varphi(z)$ and $\psi(z)$ are obtained:

$$\varphi(z) = \frac{P_c}{4\pi i\sin^2\omega_o}\left[\left(\cos 2\omega_o z + \frac{z^4-3R^4}{6R^2z}\right)\ell n\frac{t_2^2-z^2}{t_1^2-z^2} + iC\ell n\frac{t_1-z}{t_1+z} - i\bar{C}\ell n\frac{t_2-z}{t_2+z} + 2i\left(\frac{\sin 2\omega_o}{3} - \omega_o\cos 2\omega_o\right)z + \frac{2i\omega_o R^2}{z} - \frac{8i\pi R\sin^3\omega_o}{3}\right] \tag{13}$$

$$\psi(z) = -\frac{P_c}{4\pi i\sin^2\omega_o}\left[\frac{3z^4+R^4}{3z^3}\ell n\frac{t_2^2-z^2}{t_1^2-z^2} + i\bar{C}\ell n\frac{t_1-z}{t_1+z} - iC\ell n\frac{t_2-z}{t_2+z} - \frac{4i\omega_o R^4}{3z^3} + \frac{2iR^2\sin 2\omega_o}{3z} + \frac{8i\pi R\sin^3\omega_o}{3}\right] \tag{14}$$

Concerning the constant C appearing in Eqs. (13) and (14) it holds that:

$$C = \frac{4R}{3}(\cos^3\omega_o + i\sin^3\omega_o) \tag{15}$$

In order for the above obtained $\varphi(z)$ and $\psi(z)$ to provide a displacement field compatible to the demand that the disc's center must remain fixed (respecting the configuration of Fig. 3), the constant term:

$$\mathbf{D} = \frac{2P_cR\sin\omega_o}{3} \tag{16}$$

must be added to both of them in accordance to the concept of the arbitrariness of the solution (Muskhelishvili, 1963).

Substituting $\varphi(z)$ and $\psi(z)$ from Eqs. (13) and (14) in the familiar polar expression for the displacements:

$$2\mu(u_r + iu_\vartheta) = e^{-2i\vartheta}[\kappa\varphi(z) - z\overline{\varphi'(z)} - \overline{\psi(z)}] \tag{17}$$

and taking under consideration Eq. (16), closed form expressions can be obtained for the displacements in polar form. In compact form, i.e. holding for both regions I and II of Fig. 3a, these expressions read as:

$$u_r=\frac{P_c}{8\pi\mu\sin^2\omega_o}\left\{\left[\frac{(\kappa-3)r^3}{6R^2}+\frac{(\kappa+1)R^2}{2r}+\frac{3r^4-R^4}{3r^3}\right]\right.$$
$$\times\sin 2\vartheta\ell n\sqrt{\frac{(R^2+r^2)^2-(2rR\sin(\omega_o-\vartheta))^2}{(R^2+r^2)^2-(2rR\sin(\omega_o+\vartheta))^2}}$$
$$+\left[(\kappa-1)\cos 2\omega_o r+\left[\frac{(\kappa-3)r^3}{6R^2}-\frac{(\kappa+1)R^2}{2r}+\frac{3r^4+R^4}{3r^3}\right]\cos 2\vartheta\right]$$
$$\cdot\begin{cases}2\pi-\tan^{-1}\frac{R\cos\omega_o-r\sin\vartheta}{R\sin\omega_o+r\cos\vartheta}-\tan^{-1}\frac{R\cos\omega_o+r\sin\vartheta}{R\sin\omega_o-r\cos\vartheta}- & \text{region I}\\ -\tan^{-1}\frac{R\cos\omega_o-r\sin\vartheta}{R\sin\omega_o-r\cos\vartheta}-\tan^{-1}\frac{R\cos\omega_o+r\sin\vartheta}{R\sin\omega_o+r\cos\vartheta} & \\ \text{the same expression without } 2\pi & \text{region II}\end{cases}$$
$$+\frac{4(\kappa+1)R}{3}(\cos^3\omega_o\cos\vartheta+\sin^3\omega_o\sin\vartheta)$$
$$\times\ell n\sqrt{\frac{R^2+r^2-2rR\sin(\omega_o+\vartheta)}{R^2+r^2+2rR\sin(\omega_o+\vartheta)}}+\frac{4(\kappa-1)R}{3}$$
$$\cdot(\cos^3\omega_o\sin\vartheta-\sin^3\omega_o\cos\vartheta)$$
$$\cdot\begin{cases}\tan^{-1}\frac{R\cos\omega_o-r\sin\vartheta}{R\sin\omega_o-r\cos\vartheta}-\tan^{-1}\frac{R\cos\omega_o+r\sin\vartheta}{R\sin\omega_o+r\cos\vartheta} & \text{region I}\\ \text{the same expression plus } \pi & \text{region II}\end{cases}$$
$$-\frac{4(\kappa+1)R}{3}(\cos^3\omega_o\cos\vartheta-\sin^3\omega_o\sin\vartheta)$$
$$\times\ell n\sqrt{\frac{R^2+r^2+2rR\sin(\omega_o-\vartheta)}{R^2+r^2-2rR\sin(\omega_o-\vartheta)}}-\frac{4(\kappa-1)R}{3}$$
$$\cdot(\cos^3\omega_o\sin\vartheta+\sin^3\omega_o\cos\vartheta)$$
$$\cdot\begin{cases}-\tan^{-1}\frac{R\cos\omega_o-r\sin\vartheta}{R\sin\omega_o+r\cos\vartheta}+\tan^{-1}\frac{R\cos\omega_o+r\sin\vartheta}{R\sin\omega_o-r\cos\vartheta} & \text{region I}\\ \text{the same expression plus } \pi & \text{region II}\end{cases}$$
$$+\frac{2(\kappa r^2+R^2)\sin 2\omega_o}{3r}-2(\kappa-1)\omega_o\cos 2\omega_o r$$
$$\left.+2\left(\kappa+1-\frac{2R^2}{3r^2}\right)\frac{\omega_o R^2\cos 2\vartheta}{r}\right\}\qquad(18)$$

$$u_\vartheta=\frac{P_c}{8\pi\mu\sin^2\omega_o}\left\{-\left[(\kappa+1)\cos 2\omega_o r+\left[\frac{(\kappa+3)r^3}{6R^2}-\frac{(\kappa-1)R^2}{2r}\right.\right.\right.$$
$$\left.\left.\left.-\frac{3r^4+R^4}{3r^3}\right]\cos 2\vartheta\right]\cdot\ell n\sqrt{\frac{(R^2+r^2)^2-(2rR\sin(\omega_o-\vartheta))^2}{(R^2+r^2)^2-(2rR\sin(\omega_o+\vartheta))^2}}$$
$$+\left[\frac{(\kappa+3)r^3}{6R^2}+\frac{(\kappa-1)R^2}{2r}-\frac{3r^4-R^4}{3r^3}\right]\sin 2\vartheta$$
$$\cdot\begin{cases}2\pi-\tan^{-1}\frac{R\cos\omega_o-r\sin\vartheta}{R\sin\omega_o+r\cos\vartheta}-\tan^{-1}\frac{R\cos\omega_o+r\sin\vartheta}{R\sin\omega_o-r\cos\vartheta}- & \text{region I}\\ -\tan^{-1}\frac{R\cos\omega_o-r\sin\vartheta}{R\sin\omega_o-r\cos\vartheta}-\tan^{-1}\frac{R\cos\omega_o+r\sin\vartheta}{R\sin\omega_o+r\cos\vartheta} & \\ \text{the same expression without } 2\pi & \text{region II}\end{cases}$$
$$+\frac{4(\kappa+1)R}{3}(\sin^3\omega_o\cos\vartheta-\cos^3\omega_o\sin\vartheta)$$
$$\times\ell n\sqrt{\frac{R^2+r^2-2rR\sin(\omega_o+\vartheta)}{R^2+r^2+2rR\sin(\omega_o+\vartheta)}}+\frac{4(\kappa-1)R}{3}$$
$$\cdot(\sin^3\omega_o\sin\vartheta+\cos^3\omega_o\cos\vartheta)$$
$$\cdot\begin{cases}\tan^{-1}\frac{R\cos\omega_o-r\sin\vartheta}{R\sin\omega_o-r\cos\vartheta}-\tan^{-1}\frac{R\cos\omega_o+r\sin\vartheta}{R\sin\omega_o+r\cos\vartheta} & \text{region I}\\ \text{the same expression plus } \pi & \text{region II}\end{cases}$$
$$+\frac{4(\kappa+1)R}{3}(\sin^3\omega_o\cos\vartheta+\cos^3\omega_o\sin\vartheta)$$
$$\times\ell n\sqrt{\frac{R^2+r^2+2rR\sin(\omega_o-\vartheta)}{R^2+r^2-2rR\sin(\omega_o-\vartheta)}}+\frac{4(\kappa-1)R}{3}$$
$$\cdot(\sin^3\omega_o\sin\vartheta-\cos^3\omega_o\cos\vartheta)$$
$$\cdot\begin{cases}-\tan^{-1}\frac{R\cos\omega_o-r\sin\vartheta}{R\sin\omega_o+r\cos\vartheta}+\tan^{-1}\frac{R\cos\omega_o+r\sin\vartheta}{R\sin\omega_o-r\cos\vartheta} & \text{region I}\\ \text{the same expression plus } \pi & \text{region II}\end{cases}$$
$$\left.-2\left(\kappa-1+\frac{2R^2}{3r^2}\right)\frac{\omega_o R^2\sin 2\vartheta}{r}\right\}\qquad(19)$$

4. Comparative study of the displacement field for characteristic load distributions

In order to quantitatively explore the main features of the above solution two materials are considered for the disc: (a) Dionysos marble with E_D = 80 GPa and ν_D = 0.25 and (b) Poly-methyl-methacrylate (commercially known as PMMA or Plexiglass) with E_P = 3.19 GPa and ν_P = 0.36). The specimens are cylindrical discs of radius R = 0.05 m and width w = 0.01 m. Both cases are considered for the same external load equal to 11 kN. The load level was selected based on experimental results (Kourkoulis et al., 1999) indicating that for Dionysos marble the fracture stress under tensile load is equal to about 7 MPa. According to the familiar formula $\sigma_{tensile}=(P_{\rm dev})/(\pi RW)$ it corresponds (for the specific geometrical features) to a load equal to about 11 kN. Assuming for the steel jaws an elastic modulus equal to E_s = 210 GPa the "relative deformability" (i.e. the ratio of the elastic moduli of the jaws over that of the specimen) is equal to d_D = 2.63 for Dionysos marble and d_P = 65.83 for the PMMA.

The results of the present solution concerning the displacements due to the parabolic radial pressure distribution are considered in juxtaposition to the respective results of the solutions for the two loading types most widely adopted in international literature: (i) concentrated (point or line in two or three dimensions, respectively) load and (ii) uniformly distributed radial pressure.

For the point load and for $P_o=P_{\rm dev}/w$ the displacement field components are expressed (by just particularizing Muskhelishvili's (1963) general solution) as:

$$u_r=\frac{P_o}{4\pi\mu}\left[\frac{r}{R}\left(\kappa+\frac{R^4-r^4}{R^4+r^4+2r^2R^2\cos 2\vartheta}\right)+\frac{2rR(R^2\cos 2\vartheta+r^2)}{R^4+r^4+2r^2R^2\cos 2\vartheta}\right.$$
$$-(\kappa+1)\sin\vartheta\ell n\sqrt{\frac{R^2+r^2+2rR\sin\vartheta}{R^2+r^2-2rR\sin\vartheta}}$$
$$\left.+(\kappa-1)\cos\vartheta\left(\tan^{-1}\frac{R+r\sin\vartheta}{r\cos\vartheta}+\tan^{-1}\frac{R-r\sin\vartheta}{r\cos\vartheta}-\pi\right)\right]\qquad(20)$$

$$u_\vartheta=\frac{P_o}{4\pi\mu}\left[\frac{2rR(r^2-R^2)\sin 2\vartheta}{R^4+r^4+2r^2R^2\cos 2\vartheta}-(\kappa+1)\cos\vartheta\ell n\sqrt{\frac{R^2+r^2+2rR\sin\vartheta}{R^2+r^2-2rR\sin\vartheta}}\right.$$
$$\left.-(\kappa-1)\sin\vartheta\left(\tan^{-1}\frac{R+r\sin\vartheta}{r\cos\vartheta}+\tan^{-1}\frac{R-r\sin\vartheta}{r\cos\vartheta}-\pi\right)\right]\qquad(21)$$

For the uniformly distributed radial pressure, P_c, the components of the displacement field were given in closed form by Markides et al. (2010) for $P_c=P_o/2R\omega_o=P_{\rm dev}/(2Rw\omega_o)$. The three loading cases considered are schematically represented in Fig. 4.

Concerning the loading angles (contact length) for the specific load they are estimated (according to Eq. (3a)) equal to about $\omega_{o,D}=2.1^\circ$ for Dionysos marble and $\omega_{o,P}=8.8^\circ$ for PMMA.

The results of the analysis for the radial displacements, u_r, along the disc's periphery are plotted in Fig. 5 while those for the transverse (hoop), u_θ, displacements are plotted in Fig. 6. As it is seen from Fig. 5 all three loading types (parabolic, uniform and point load) yield more or less identical results for the radial displacements for the major part of the disc's perimeter (small figures embedded in Fig. 5(a,b)). u_r is positive (directed outwards from the disc) in the region $0^\circ<\theta<\theta_{cr}\approx 45^\circ$ for marble (Fig. 5(a)) and in the region $0^\circ<\theta<\theta_{cr}=50^\circ$ for PMMA (Fig. 5(b)) and becomes negative (directed inwards to the disc) in the region $\theta_{cr}<\theta<90^\circ$. Significant differences between the results corresponding to the three load cases appear only while closely approaching the loaded rim. Indeed for $90^\circ-\omega_o<\theta<90^\circ$ the solutions start deviating from each other. The radial displacement due to the point load gradually exceeds the respective values due to the distributed loads and as θ approaches 90° u_r becomes infinite. On the contrary the

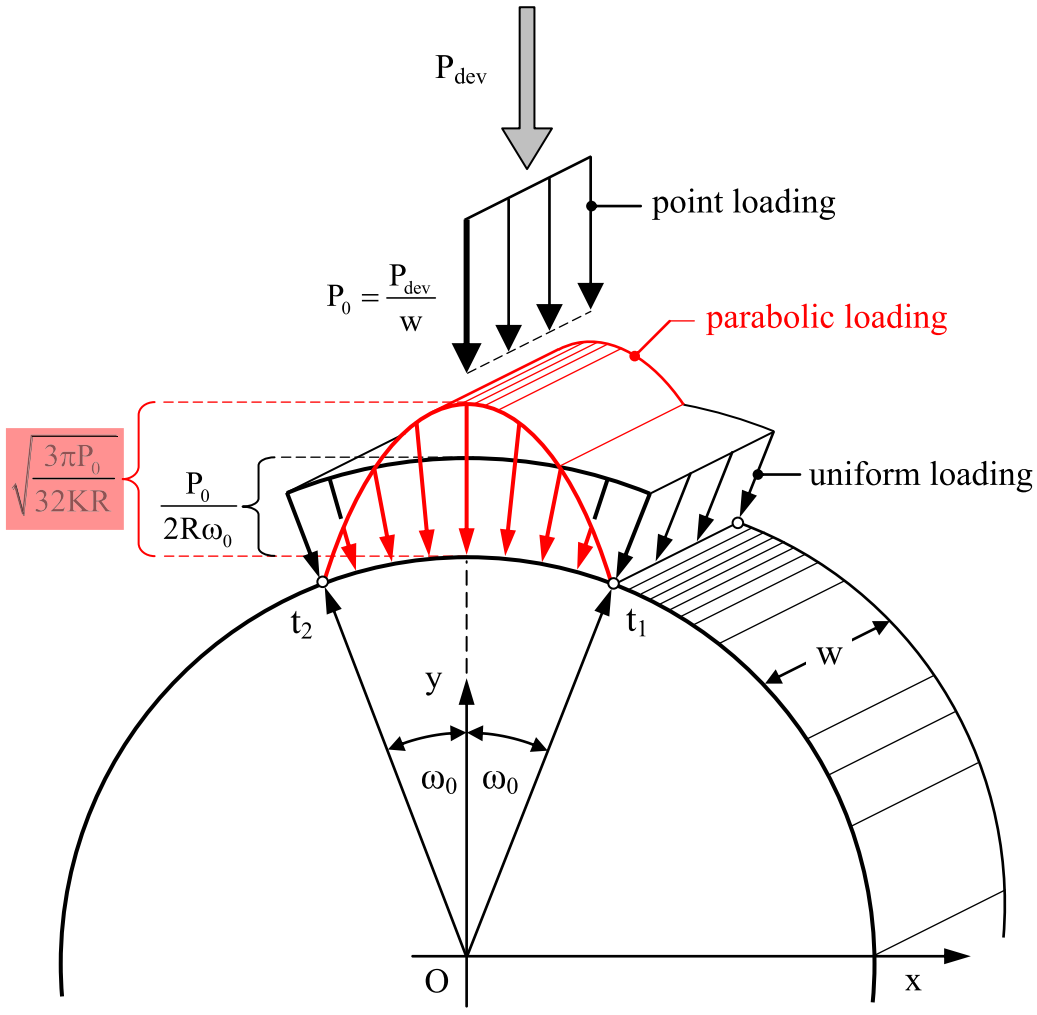

Fig. 4. The loading types comparatively considered.

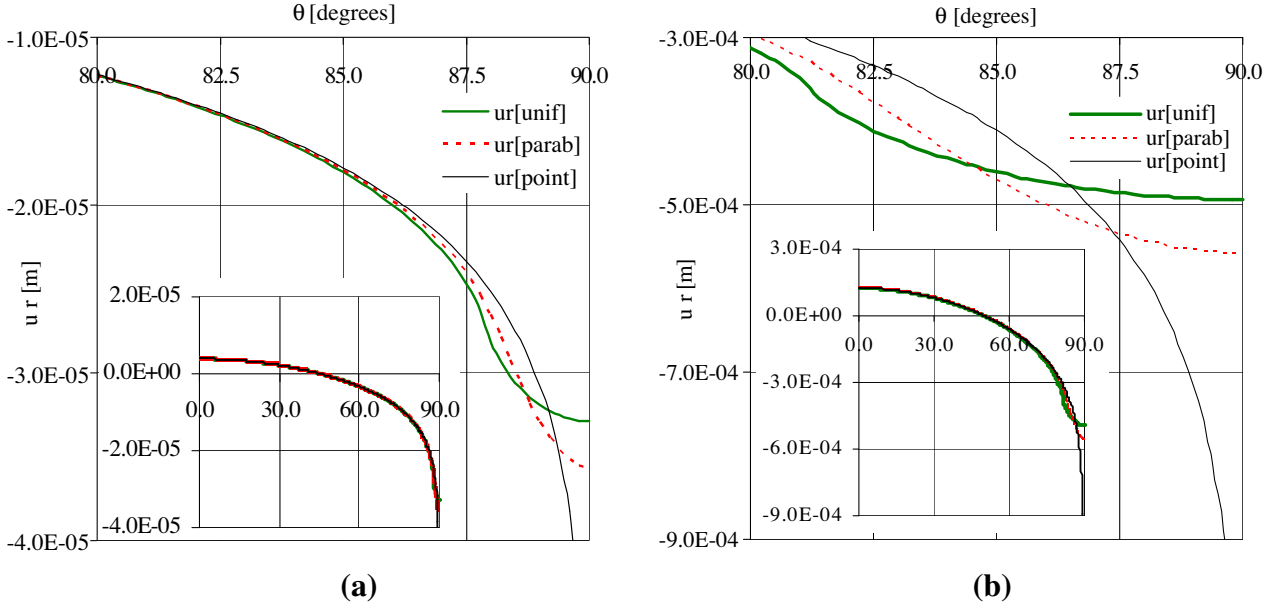

Fig. 5. The variation of the radial displacement, u_r, along the disc's periphery for an external load equal to $P = 10$ kN for (a) Marble and (b) PMMA.

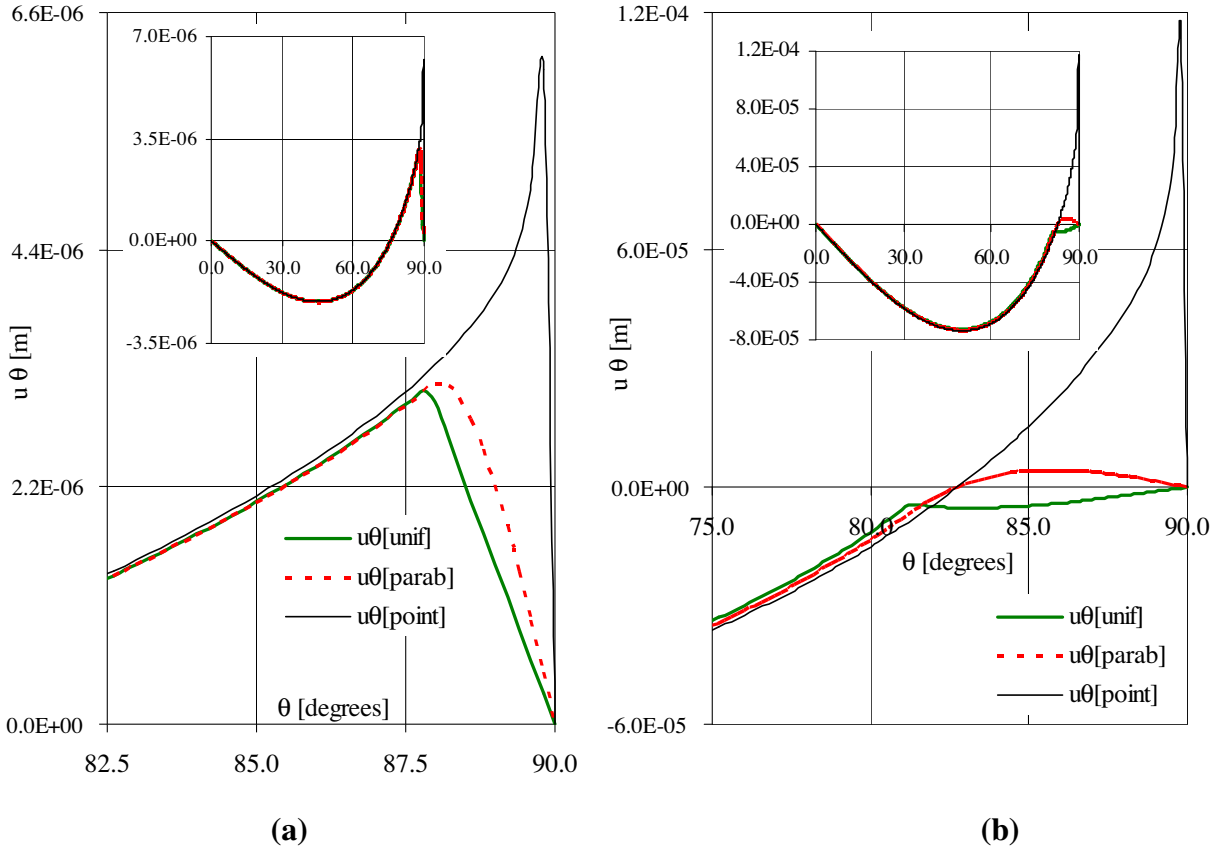

Fig. 6. The variation of the transverse (hoop) displacement, u_θ, along the disc's periphery for an external load equal to $P = 10$ kN for (a) Marble and (b) PMMA.

displacements due to the uniform and parabolic load distribution remain finite even for $\theta = 90°$. As it is perhaps expected for $\theta = 90°$ the radial displacement u_r for the parabolic load exceeds that for the uniform load both for Dionysos marble and PMMA. The absolutely maximum values of the radial displacement due to the distributed loads vary between 3.3×10^{-5} m and 3.6×10^{-5} m for marble and between 4.9×10^{-4} m and 5.5×10^{-4} m for PMMA; in other words there is a difference higher than one order of magnitude.

Concerning now the transverse (hoop) displacements, u_θ, it is seen from Fig. 6 that the solutions for the three loading types considered are again almost identical for the major part of the disc's periphery for both materials (small figures embedded in Fig. 6(a,b)). Differences are again detectable only as one approaches the loaded rims. In the case of marble, loaded by either uniform or parabolic load distributions, the transverse displacements are negative for $0 < \theta < 77.2°$ and then they become positive reaching a maximum value at an angle $\theta \approx 88°$ (the end point of the loaded rim), equal to about 3.1×10^{-6} m (Fig. 6(a)). Then the displacements start decreasing reaching zero at $\theta = 90°$. The displacements due to the point load significantly exceed those of both the uniform and the parabolic load distributions reaching their maximum value (equal to about 6.1×10^{-6} m) at an angle tending to $\theta = 90°$. For PMMA (Fig. 6(b)) the overall behaviour is almost identical, from a qualitative point of view. The main difference is the behaviour for the uniform load distribution: The transverse displacements are constantly negative for the whole disc's periphery.

The last conclusion becomes very important in case one intends to consider friction effects between the disc and the loading platens. Indeed, as it schematically shown in Fig. 7, the tendency motion for marble in the loaded rim is inwards for both load distributions (uniform and parabolic) and therefore friction is directed outwards (Fig. 7a). On the contrary for PMMA the tendency motion for the parabolic distribution (Fig. 7b1) is again inwards (therefore friction is directed outwards) while for the uniform distribution (Fig. 7b2) the tendency motion is outwards (and therefore friction is directed inwards). It was found that increasing further the load intensity (increasing also the extent of the loaded rim) the inwards motion tendency for the parabolic load is inverted and the motion is directed outwards for both uniform and parabolic distributions. It can be said therefore that it is not possible to a-priori decide about the direction of friction forces based exclusively on the relative deformability of disc and platens (Lavrov and Vervoort, 2002) but rather it is imperative to know both the loading type and also the intensity of the external load.

5. Experimental study

5.1. Experimental procedure

In order to further assess the above analytic solution standardized Brazilian-disc tests were carried out. The components of the displacement-field developed were measured using a novel 3D digital image correlation (DIC) system by LIMESS. DIC is a contactless video-based technique the theoretical foundation of which is dated back to '80s (Chu et al., 1985). A thorough description of the background of DIC technique and its broad applications field are given by Sutton et al. (2000). The main requirement that has to be met for the successful use of DIC is that the specimen surface must be covered with a speckle pattern which will provide the necessary features for the matching process.

The specimens were cylindrical discs (radius $R = 0.05$ m, thickness $w = 0.01$ m) made from PMMA. The choice of PMMA was

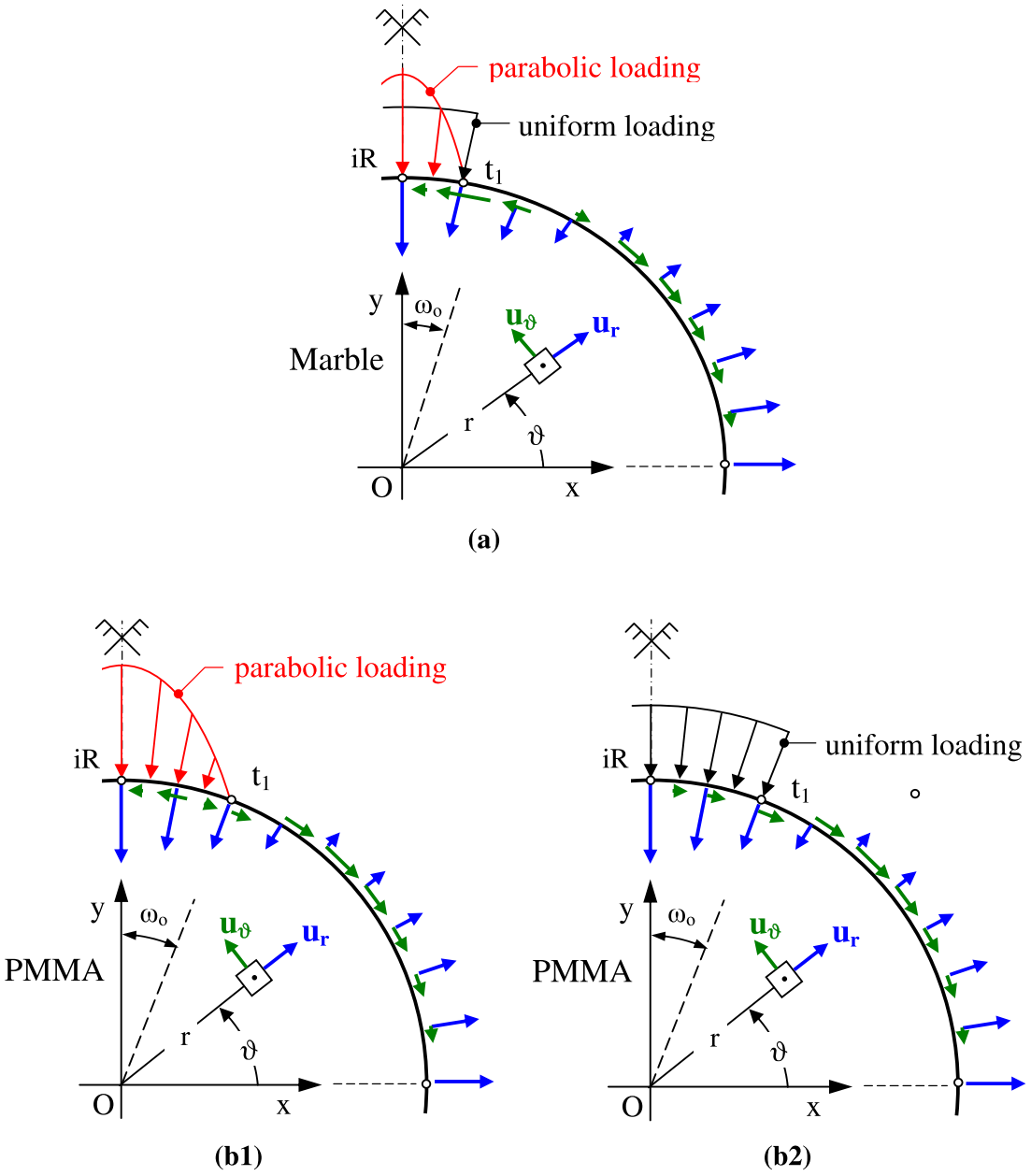

Fig. 7. Schematic representation of the displacements' direction for (a) Marble and (b) PMMA under parabolic (b1) and uniform (b2) radial pressure distribution.

based on the fact that its mechanical behaviour approaches in a satisfactory manner that of a linear elastic material. After mechanically shaping the specimens one of their lateral surfaces was painted with white paint and then it was sprayed with a black aerosol until a uniform speckle pattern was produced (Fig. 8a).

Six experiments were executed using the standardized ISRM apparatus mounted to a 50 kN electromechanical INSTRON loading frame (Fig. 8b). A semi-spherical head interposed between the upper jaw and the moving traverse of the frame ensured normality. The experiments were quasi-static under displacement control mode at a rate of 0.01 mm/min. The resulting compression force was measured using a 25 kN load cell calibrated with a verified Wykeham Farrance compression ring of sensitivity 10.62 N. The response of the cell was linear throughout the whole load range of interest and the deviation did not exceed 0.2%. In addition the displacement rate was calibrated using a verified high mag micrometric calibrator. Again the response was linear and the deviation did not exceed 0.4%.

The "undeformed" specimen state was considered when it was placed within the jaws before applying any external load. Therefore in the "undeformed" state the specimen was in fact loaded by the own weight of the upper jaw which is 58.85 N. During loading, images of the deformed specimen were taken for load levels ranging from 1 kN to 20 kN with an 1 kN interval. The maximum load was kept relatively far from the fracture load to ensure that the material indeed behaves linearly at least at regions far from the loaded rim.

The scattering between the results of the six tests concerning the displacements was almost negligible.

5.2. Experimental results

The variation of the Cartesian components of the displacement field, u_x and u_y, all over the specimen's surface for a load level equal to 20 kN are shown in Fig. 9. In both figures the rigid body displacements have been removed, using appropriate software. Then, in

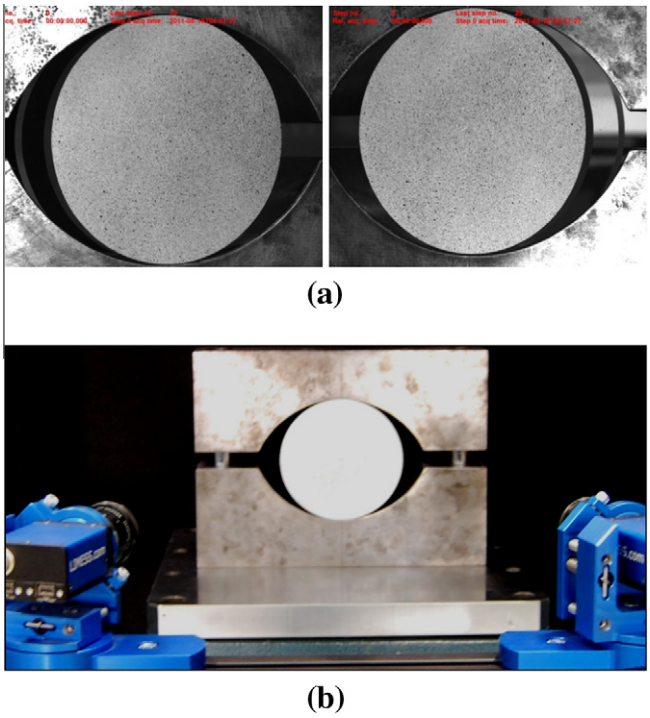

Fig. 8. (a) Typical specimen as it is seen from the two cameras of the DIC system after the speckle pattern is produced. (b) Overview of the experimental set-up.

order for the analytically obtained results to be directly comparable with the experimental ones, the latter were "corrected" by removing the displacements corresponding to the vertical motion of the x-axis (horizontal) of symmetry. Indeed according to the theoretical configuration the load is applied symmetrically on both jaws and therefore x-axis remains fixed. On the contrary during the experimental procedure only the upper jaw is moving (downwards) and therefore the displacements along y-axis are not symmetric with respect to the horizontal axis of symmetry unless the above mentioned "correction" is realized. From Fig. 9, besides the (expected) symmetry of u_x-component with respect to y-axis and that of u_y-component with respect to x-axis, some interesting quantitative data are obtained concerning the maximum values of the displacements reached: for the u_x-component (Fig. 9(a)) the extreme values are of the order of 0.25 mm while for the u_y-component (Fig. 9(b)) the respective value slightly exceeds 1.0 mm, i.e. it is about five times higher from u_x.

The variation of the displacement components along the radii with $\theta = 0^\circ$ and $\theta = 90^\circ$ (normalized over the disc's radius, R) are plotted in Fig. 10, together with the respective results of the analytic solution, introduced above for the parabolic radial pressure distribution. The plots are again realized for a load level equal to 20 kN. The agreement between theory and experiment is almost excellent for the displacement developed along the $\theta = 0^\circ$ radius (i.e. for the $u_r \equiv u_x$ component). Concerning the displacement along the $\theta = 90^\circ$ radius (i.e. for the $u_r \equiv u_y$ component) it is observed that the agreement is qualitatively satisfactory, however some quantitative discrepancies appear. Namely, the experimental results systematically exceed the analytic ones. The maximum deviation, equal to about 8%, is observed for $r \to R$. This discrepancy could be attributed to the assumption of linear elasticity adopted in the analytic solution: In the immediate vicinity of the area where contact between disc and platen is realized the material does not behave linearly (even for low level loads) and therefore the actual displacements are higher than those predicted by the analytic solution.

The polar variation of both the radial and the transverse (hoop) displacement components along the disc's periphery is plotted in Fig. 11. Only the first quadrant ($0^\circ < \theta < 90^\circ$) is considered due to the double symmetry of the displacements field (with respect to both x- and y-axes). In fact the plots are realized along a quarter of a circle of radius $r = 0.95$ R. This is dictated by practical restrictions since as $r/R \to 1$ the accuracy of the DIC technique is downgraded by optical effects due to the geometric discontinuity at $r = R$ (the disc is thinner than the jaws). It is seen that u_θ is negative all along the specific path while u_r changes sign at an angle θ between 46° and 50°. The qualitative agreement between theory and experiment is very good. From the quantitative point of view some deviations appear. For u_θ the maximum deviation is observed around $\theta = 45^\circ$ and it varies around 18%. The experimentally measured values are slightly, but systematically, higher than the respective theoretical ones. Concerning u_r the maximum deviation is observed at $\theta = 90^\circ$ and it varies around 8%.

Based on the displacements one can obtain the respective strain- and (knowing the constitutive law) stress-fields. In this direction the strain components developed along the $\theta = 0^\circ$ and $\theta = 90^\circ$ radii are plotted in Figs. 12 and 13 as obtained from the experimentally measured displacements. In the same figures the analytically obtained strain components are plotted for comparison. The analytic solution is based on the stress field developed in a Brazilian disc under parabolic radial pressure, as proposed recently by Markides and Kourkoulis (in press), using Hooke's generalized law and assuming that PMMA behaves as a linear elastic material. The components for the stress field are included in Appendix I. It is mentioned, also, that the scattering of the experimentally obtained strains is considerably higher from that exhibited by the results for the displacements. This can be attributed to the fact that the strains are obtained indirectly by differentiating the results for the displacements. It is expected that slope measurements are much more sensitive compared to those of displacements. Finally it is recalled that the experimental results are, as previously, restricted in the $0 < r/R < 0.95$ region, for practical reasons related to the application of the DIC technique.

It is seen from Fig. 12 ($\theta = 0^\circ$) that the agreement between theory and experiment is very satisfactory both qualitatively and quantitatively. Especially for the radial strain, ε_{rr}, the discrepancies are almost zero. For the transverse (hoop) strain, $\varepsilon_{\theta\theta}$, the maximum deviation between the experimental and the analytic results is measured at $r/R \approx 0.5$ and varies around 20%. Similar conclusions are drawn from Fig. 13 ($\theta = 90^\circ$). Again the agreement for ε_{rr} is excellent while for $\varepsilon_{\theta\theta}$ some deviations appear for $r/R > 0.50$. These deviations are maximized at about $r/R \approx 0.83$ and they are of the order of 15%.

5.3. The contact length

As a last step of the experimental study an attempt was undertaken to assess the validity of Eq. (1b) (or equivalently Eq. (3a)), providing the extent of the contact length, or equivalently the contact angle, ω_o. Theoretically speaking the end-points of the contact rim could be defined as the points where the contact stress becomes zero. Obviously this direct definition cannot be used in experimental practice since stresses cannot be measured directly and even more the contact stresses cannot be isolated from the remaining components of the stress field. Therefore one should accept a different principle which could be applied experimentally. It appears reasonable to assume that at the end-points of the contact rim the polar distributions of the displacements and strains should exhibit either changes of their curvature (points of inflection) or extreme values (local or global), respectively.

The analytically determined polar distribution of the displacement components along the disc's periphery is plotted in Fig. 14, for an overall load of 20 kN. Attention is focused in the region very closely to the end points of the loaded rim. The dotted lines

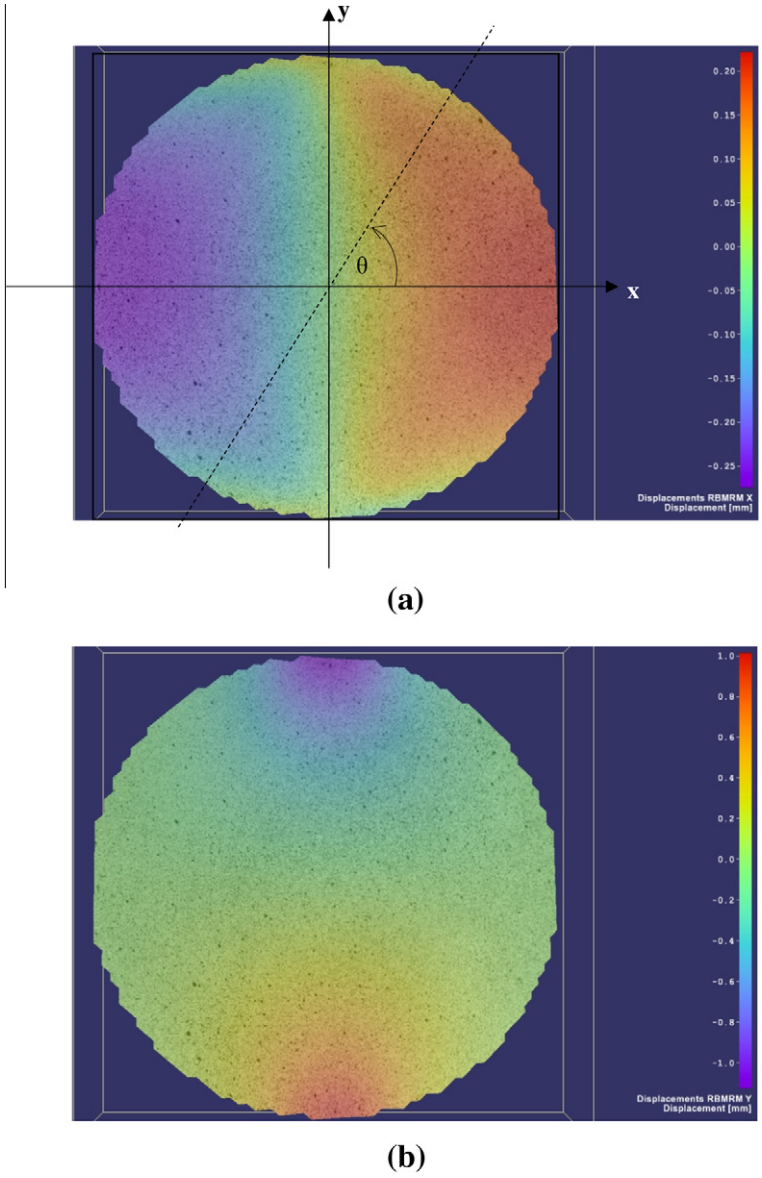

Fig. 9. The field of (a) horizontal, u_x- and (b) vertical u_y- displacements for a load level equal to 20 kN. The rigid body movement has been removed.

represent the critical angle θ_o as obtained from the theoretically calculated (using Eq. (3a)) contact arc ω_o (for an external load equal to 20 kN it is found that $\omega_o = 11.88°$). It is seen that both $u_\theta = u_\theta(\theta)$ and $u_r = u_r(\theta)$ curves exhibit their points of inflection very close to $\theta_o = 90° - \omega_o = 78.12°$. In fact for u_θ the point of inflection is at $\theta \approx 76.5°$ while for u_r at $\theta \approx 80.5°$ (doubly dotted lines in Fig. 14(a,b)).

Taking into account the above results the experimentally obtained polar distribution of the strain components along the disc's periphery is plotted in Fig. 15 for the $70° < \theta < 90°$ interval. It is seen from this figure that in the relatively narrow band $76.5° < \theta < 80.5°$ around $\theta_o = 78.12°$, defined by the above points of inflection (dashed rectangle in Fig. 15) the curves corresponding to the normal strains exhibit their points of inflection while the curve corresponding to the shear strain exhibits its global minimum.

It should be emphasized however that this is a purely experimental observation which is accurate within a given degree of approximation. In addition it can be seen that around $\theta = 78.12°$ the polar distribution of strains is strongly fluctuating and all three strain components exhibit various characteristic points (extrema and points of inflection) which could be used as critical quantities for the determination of ω_o.

Considering the above results it can be safely concluded that in a first approximation the contact length can be equally well estimated experimentally either from the points of inflection of the polar distributions of displacements and normal strains or from the points of global minimum of shear strain's polar distribution. In this context the theoretically predicted contact length, ω_o, is plotted in Fig. 16, versus the externally applied load. In the same figure the experimentally measured contact length is plotted considering its end points either as the points of inflection of the transverse (hoop) displacement's distribution or the points corresponding to the global extremum of the shear strain's distribution (both realized along the disc's periphery).

The qualitative agreement is indeed excellent, while from a quantitative point of view the approach based on shear strain seems to slightly overestimate the magnitude of the contact length while the approach based on the transverse displacement slightly underestimates it. The maximum deviation for the approach based on displacements is about 20% (for a load equal to 12 kN) while for that based on shear strain is about 10% (for a load equal to 10 kN).

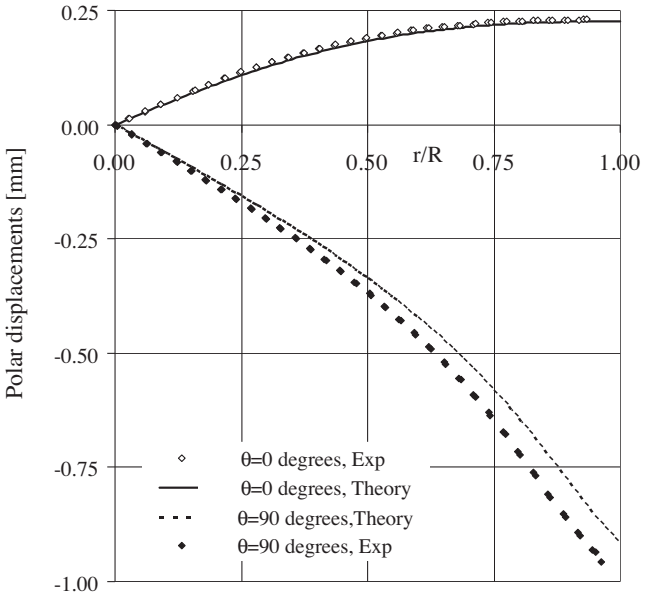

Fig. 10. Experimentally measured and analytically predicted displacements along the $\theta = 0^\circ$ and $\theta = 90^\circ$ radii, for PMMA and external load 20 kN.

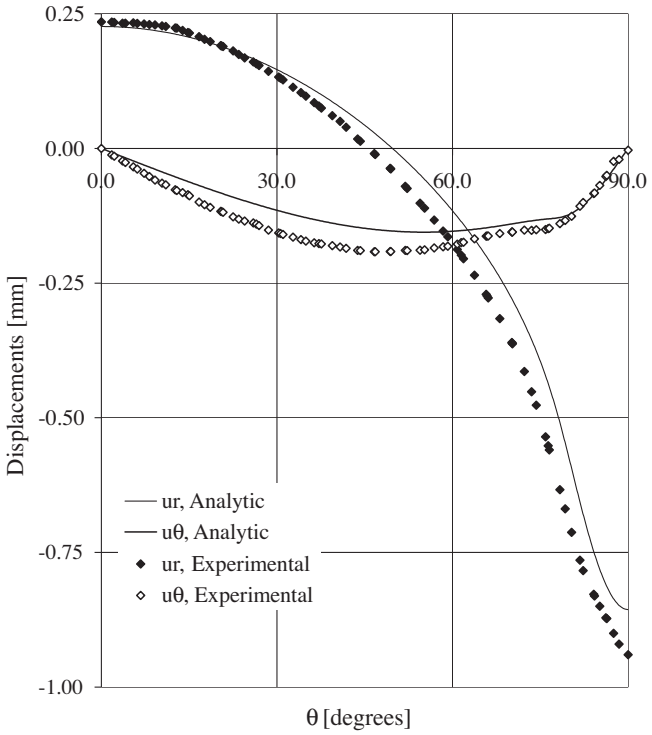

Fig. 11. Experimentally measured and analytically predicted displacements along a quarter of circle with $r = 0.95$ R, for PMMA and external load 20 kN.

6. Discussion

An analytic, closed form, solution for the displacement field developed in a Brazilian disc subjected to a parabolic radial pressure distribution along two symmetric arcs of its periphery was introduced. The specific loading type was adopted based on a recent study of the jaw-disc contact problem (Kourkoulis et al., 2012). Moreover the pressure was applied along a contact rim the length of which is not arbitrarily predefined but rather along

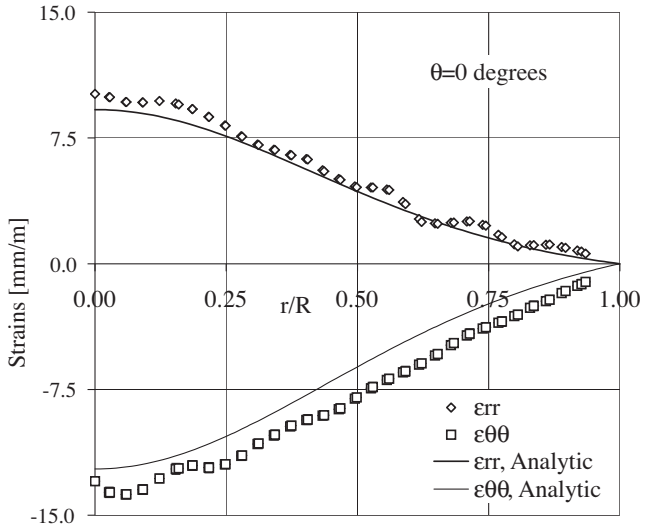

Fig. 12. Experimentally measured and analytically predicted strains along the $\theta = 0^\circ$ radius for PMMA and external load 20 kN.

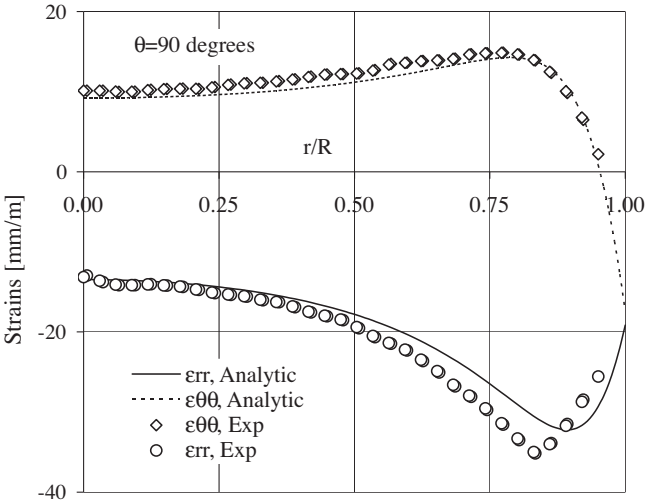

Fig. 13. Experimentally measured and analytically predicted strains along the $\theta = 90^\circ$ radius for PMMA and external load 20 kN.

a rim the length of which depends on the elastic properties of the disc's and jaw's materials, the geometry and the level of the external load. The solution was assessed using the results of a short series of experiments in which the displacements were measured using the DIC technique.

The comparative study of three different load types (uniform and parabolic variation of the radial pressure and point load) indicated that as long as one focuses attention at the center of the disc all three solutions yield identical results. Serious discrepancies appear only as one approaches the jaw-disc interface. Ignoring the actual load variation in this region yields erroneous results since the differences are not only quantitative: For the transverse (hoop) displacements it was indicated that the loading type adopted influences their direction or in other words the direction of the friction forces inevitably developed at the disc-jaw interface in case they are made from materials with different deformability. From a physical point of view this difference could be attributed to the fact that a load distribution more intense near the vertex point (the case of parabolic loading) forces material points close to the vertex to move (shrink) inwards (u_θ positive). This tendency

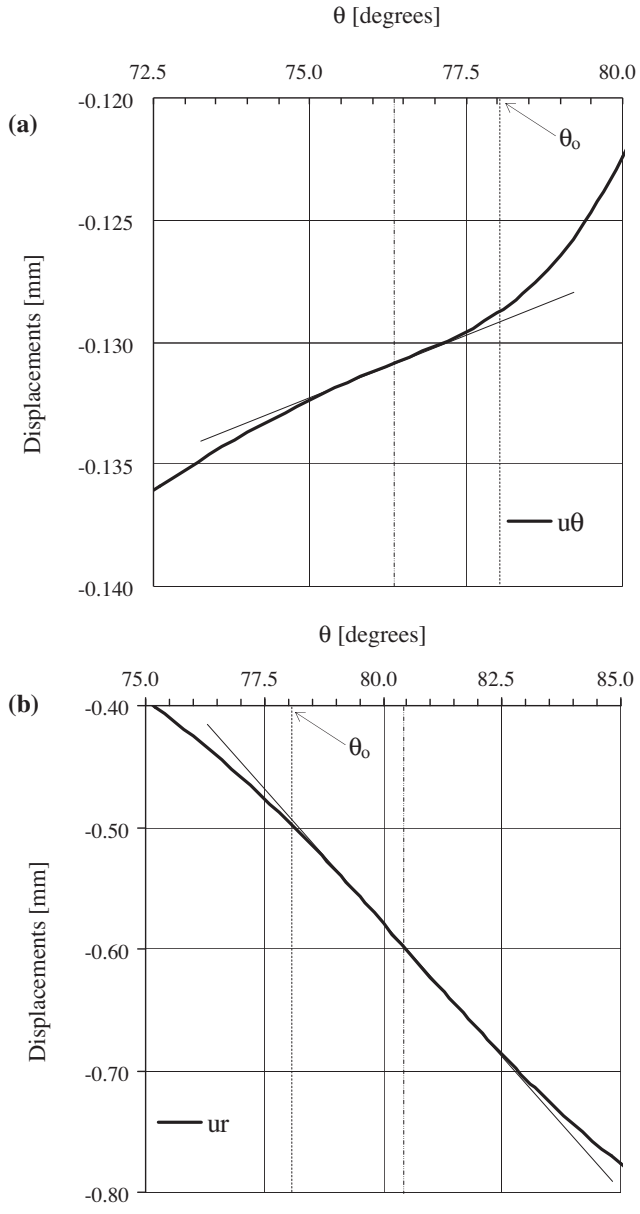

Fig. 14. Analytically calculated transverse (a) and radial (b) displacements in the vicinity of the disc-jaw interface for an overall load of 20 kN. Dotted lines represent the theoretically calculated contact angle ω_o while double dotted ones the points of inflection.

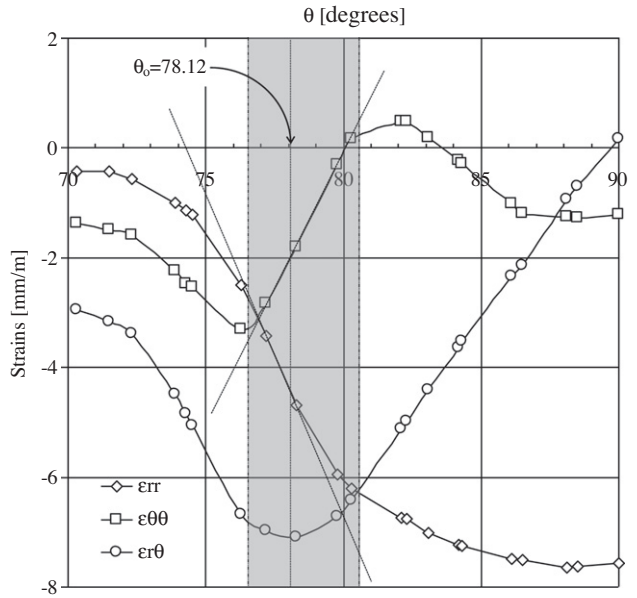

Fig. 15. Experimentally measured strains along the $r/R = 0.95$ quarter of a circle. The dashed area includes the points of inflection and the points of global extrema.

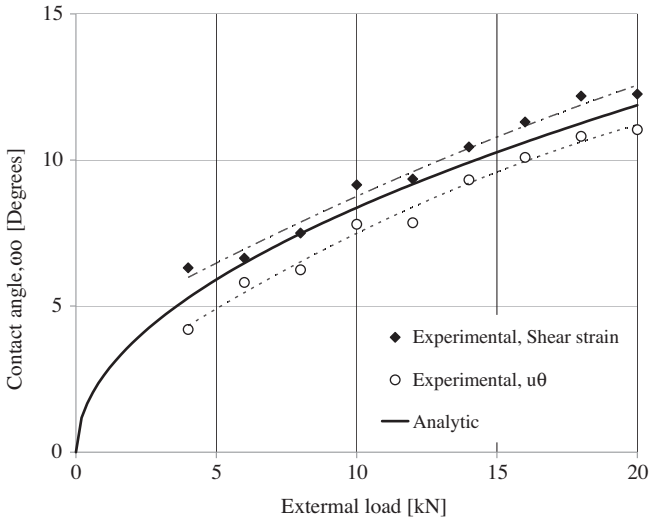

Fig. 16. Experimentally measured and analytically calculated contact angle.

slowly reduces along the contact rim changing to an outwards moving tendency (u_θ negative). On the other hand a relatively smooth load around the vertex point (the case of uniformly distributed loading) does not cause such an inwards contraction of the material points but rather it causes a monotonic increasing outwards motion tendency (u_θ constantly positive) along the contact rim as well as out of it.

It is also important to note that the direction of the transverse displacements along the loaded rim depends also on the load level indicating that the direction of friction developed inverses its direction during the loading procedure.

The last point is crucial in case friction forces are to be considered at the disc-jaw interface: contrary to the common practice, according to which the direction of friction is dictated exclusively by the relative deformability of the disc's and jaw's materials (Lavrov and Vervoort, 2002), it was revealed that an a-priori decision about the direction of friction forces is not permitted: before a decision is made one must take into account the loading type and the intensity of the external load.

Clearly friction is among the points that should be further studied. The displacements here obtained could be used (assuming for example that u_θ is somehow related to friction) to solve the respective problem with both radial and tangential loads along the loaded rim. The main question to be answered is the relation between radial and tangential loads since a typical Coulomb law is inadequate.

7. Conclusions

The experimental study indicated that the solution here introduced for the displacement field approaches satisfactory the actual field developed in the disc under parabolically varying radial pressure. The same is true for the strain field which was here determined analytically based on an earlier introduced solution for

the stress field. Some discrepancies appearing can be attributed either to the linear elastic assumption adopted in the theoretical analysis or to the "small-angle" approximation (Eq. (3a)) which for PMMA is perhaps on the borderline of its validity.

Concerning the analytic formula for the determination of the contact length it must be emphasized from the very beginning that there is not a standardized experimental technique for measuring the contact angle. Both approaches adopted here (based on the points of inflection of the displacements' polar distribution and on the points of global extrema of the shear strain's polar distribution) seem to be satisfactory. It can not be yet definitely indicated which one is better. Of course it could be said that since displacements are directly measured (contrary to strains which are indirectly calculated by differentiation) they are preferable, although they underestimate (slightly but systematically) the values predicted by the analytic solution. Clearly the specific point should be further studied using specimens made from different (more brittle) materials, like marble or other rock-like geomaterials and concrete.

Before concluding it is emphasized again that the solution presented for the displacement field is caused by a parabolically varying radial pressure distribution which is not identical to the actual circular one (Eq. (1a)) obtained from the solution of the respective contact problem. The reason is that analytic closed form expressions from the displacement field cannot be obtained for the distribution of Eq. (1a). On the other hand the parabolic distribution chosen ((Eq. (2))) not only constitutes an efficient substitute (reducing mathematical complexities) substitute but perhaps it approaches reality better: Indeed the cyclic distribution of P is obtained for an approximately straight contact segment $(-\ell, +\ell)$ according to Muskhelishvili's (1963) approach for locally flattened boundaries. It appears therefore that for an initially circular contact region $(-\ell, +\ell)$ a parabolic distribution (of slightly increased intensity at the vertex and slightly reduced intensity around the end points of the loaded rim) could be more reasonable compared to the perfectly circular. Such a conclusion seems to be supported by a preliminary numerical study of the problem based on the finite element method. In any case although the difference between the two distributions (parabolic and circular) is very small it is possible that the results obtained could be of reduced accuracy in the immediate vicinity of the end points of the distribution. Clearly the specific point must be further studied.

Appendix A

The stress field in a Brazilian disc loaded by a parabolic radial pressure distribution is given in polar coordinates as follows (Markides and Kourkoulis, in press):

$$\begin{aligned}\sigma_{rr}=&\frac{P_c}{4\pi\sin^2\omega_o}\left\{\left(\frac{R^2-r^2}{r^2}\right)^2\frac{\sin2\vartheta}{2}\ell n\frac{(R^2+r^2)^2-(2rR\sin(\omega_o-\vartheta))^2}{(R^2+r^2)^2-(2rR\sin(\omega_o+\vartheta))^2}\right.\\&+\frac{4\omega_oR^2(R^2-2r^2)}{r^4}\cos2\vartheta+\left(\frac{r^4-R^4+2r^2R^2}{r^4}\cos2\vartheta+2\cos2\omega_o\right)\\&\cdot\left\langle\begin{array}{l}2\pi-\tan^{-1}\frac{R\cos\omega_o-r\sin\vartheta}{R\sin\omega_o+r\cos\vartheta}-\tan^{-1}\frac{R\cos\omega_o+r\sin\vartheta}{R\sin\omega_o-r\cos\vartheta}-\\-\tan^{-1}\frac{R\cos\omega_o-r\sin\vartheta}{R\sin\omega_o-r\cos\vartheta}-\tan^{-1}\frac{R\cos\omega_o+r\sin\vartheta}{R\sin\omega_o+r\cos\vartheta}\end{array}\right\}\ region\ I\\&\text{the same expression without } 2\pi\qquad region\ II\\&+(R^2-r^2)\left[\left(\frac{r^2}{R^2}\sin4\vartheta+2\cos2\omega_o\sin2\vartheta\right)\left(\frac{-R^2\cos2\omega_o-r^2\cos2\vartheta}{(R^2+r^2)^2-(2rR\sin(\omega_o+\vartheta))^2}\right.\right.\\&\left.+\frac{R^2\cos2\omega_o+r^2\cos2\vartheta}{(R^2+r^2)^2-(2rR\sin(\omega_o-\vartheta))^2}\right)-\left(\frac{r^2}{R^2}\cos4\vartheta+2\cos2\omega_o\cos2\vartheta+\frac{R^2}{r^2}\right)\\&\left.\left.\left(\frac{R^2\sin2\omega_o-r^2\sin2\vartheta}{(R^2+r^2)^2-(2rR\sin(\omega_o+\vartheta))^2}+\frac{R^2\sin2\omega_o+r^2\sin2\vartheta}{(R^2+r^2)^2-(2rR\sin(\omega_o-\vartheta))^2}\right)\right]-4\omega_o\cos2\omega_o\right\}\end{aligned}\tag{1}$$

$$\begin{aligned}\sigma_{\vartheta\vartheta}=&\frac{P_c}{4\pi\sin^2\omega_o}\left\{\frac{2r^6-R^6-r^4R^2}{2r^4R^2}\sin2\vartheta\ell n\frac{(R^2+r^2)^2-(2rR\sin(\omega_o-\vartheta))^2}{(R^2+r^2)^2-(2rR\sin(\omega_o+\vartheta))^2}\right.\\&-\frac{4\omega_oR^4}{r^4}\cos2\vartheta+\left(\frac{2r^6+R^6-r^4R^2}{r^4R^2}\cos2\vartheta+2\cos2\omega_o\right)\\&\cdot\left\langle\begin{array}{l}2\pi-\tan^{-1}\frac{R\cos\omega_o-r\sin\vartheta}{R\sin\omega_o+r\cos\vartheta}-\tan^{-1}\frac{R\cos\omega_o+r\sin\vartheta}{R\sin\omega_o-r\cos\vartheta}-\\-\tan^{-1}\frac{R\cos\omega_o-r\sin\vartheta}{R\sin\omega_o-r\cos\vartheta}-\tan^{-1}\frac{R\cos\omega_o+r\sin\vartheta}{R\sin\omega_o+r\cos\vartheta}\end{array}\right\}\ region\ I\\&\text{the same expression without } 2\pi\qquad region\ I\\&(R^2-r^2)\left[\left(\frac{r^2}{R^2}\sin4\vartheta+2\cos2\omega_o\sin2\vartheta\right)\left(\frac{-R^2\cos2\omega_o-r^2\cos2\vartheta}{(R^2+r^2)^2-(2rR\sin(\omega_o+\vartheta))^2}\right.\right.\\&\left.+\frac{R^2\cos2\omega_o+r^2\cos2\vartheta}{(R^2+r^2)^2-(2rR\sin(\omega_o-\vartheta))^2}\right)-\left(\frac{r^2}{R^2}\cos4\vartheta+2\cos2\omega_o\cos2\vartheta+\frac{R^2}{r^2}\right)\\&\left.\left.\cdot\left(\frac{R^2\sin2\omega_o-r^2\sin2\vartheta}{(R^2+r^2)^2-(2rR\sin(\omega_o+\vartheta))^2}+\frac{R^2\sin2\omega_o+r^2\sin2\vartheta}{(R^2+r^2)^2-(2rR\sin(\omega_o-\vartheta))^2}\right)\right]-4\omega_o\cos2\omega_o\right\}\end{aligned}\tag{2}$$

$$\begin{aligned}\sigma_{r\vartheta}=&\frac{P_c(R^2-r^2)}{4\pi\sin^2\omega_o}\left[\frac{r^4-R^4}{2r^4R^2}\cos2\vartheta\ell n\frac{(R^2+r^2)^2-(2rR\sin(\omega_o-\vartheta))^2}{(R^2+r^2)^2-(2rR\sin(\omega_o+\vartheta))^2}\right.\\&+\frac{4\omega_oR^2}{r^4}\sin2\vartheta-\frac{r^4+R^4}{r^4R^2}\sin2\vartheta\\&\left\langle\begin{array}{l}2\pi-\tan^{-1}\frac{R\cos\omega_o-r\sin\vartheta}{R\sin\omega_o+r\cos\vartheta}-\tan^{-1}\frac{R\cos\omega_o+r\sin\vartheta}{R\sin\omega_o-r\cos\vartheta}-\\-\tan^{-1}\frac{R\cos\omega_o-r\sin\vartheta}{R\sin\omega_o-r\cos\vartheta}-\tan^{-1}\frac{R\cos\omega_o+r\sin\vartheta}{R\sin\omega_o+r\cos\vartheta}\end{array}\right\}\ region\ I\\&\text{the same expression without } 2\pi\qquad region\ II\\&+\left(\frac{r^2}{R^2}\sin4\vartheta+2\cos2\omega_o\sin2\vartheta\right)\left(\frac{R^2\sin2\omega_o-r^2\sin2\vartheta}{(R^2+r^2)^2-(2rR\sin(\omega_o+\vartheta))^2}\right.\\&\left.+\frac{R^2\sin2\omega_o+r^2\sin2\vartheta}{(R^2+r^2)^2-(2rR\sin(\omega_o-\vartheta))^2}\right)+\left(\frac{r^2}{R^2}\cos4\vartheta+2\cos2\omega_o\cos2\vartheta+\frac{R^2}{r^2}\right)\\&\left.\times\left(\frac{-R^2\cos2\omega_o-r^2\cos2\vartheta}{(R^2+r^2)^2-(2rR\sin(\omega_o+\vartheta))^2}+\frac{R^2\cos2\omega_o+r^2\cos2\vartheta}{(R^2+r^2)^2-(2rR\sin(\omega_o-\vartheta))^2}\right)\right]\end{aligned}\tag{3}$$

References

ASTM, 1988. Standard method for splitting tensile strength of intact rock core specimens. 04.08, pp. 471–475.

Akazawa, T., 1943. New test method for evaluating internal stress due to compression of concrete (the splitting tension test) (Part 1). J. Japan Soc. Civil Eng.

Carneiro, F.L.L.B., 1943. A new method to determine the tensile strength of concrete. In: Proceedings of the 5th Meeting of the Brazilian Association for Technical Rules, 3d. Section, 16 September 1943, pp. 126–129 (in Portuguese).

Chu, T., Ranson, W., Sutton, M., 1985. Applications of digital-image-correlation techniques to experimental mechanics. Exp. Mech. 25, 232–244.

Claesson, J., Bohloli, B., 2002. Brazilian test: stress field and tensile strength of anisotropic rocks using an analytical solution. Int. J. Rock. Mech. Mining Sci. 39, 991–1004.

Colback, P.S.B., 1967. An analysis of brittle fracture initiation and propagation in the Brazilian test. In: Proceedings of the 1st Congress of ISRM, pp. 385–391.

Fairbairn, E.M.R., Ulm, F.-J., 2002. A tribute to engineer and scientist who invented the Brazilian test. Mater. Struct. 35, 195–196, Fernando L.L.B. Carneiro (1913–2001).

Fairhurst, C., 1964. On the validity of the 'Brazilian' test for brittle materials. Int. J. Rock. Mech. Min. Sci. 1, 535–546.

Hondros, G., 1959. The evaluation of Poisson's ratio and the modulus of materials of a low tensile resistance by the Brazilian (indirect tensile) test with particular reference to concrete. Aust. J. Appl. Sci. 10, 243–268.

Hooper, J.A., 1971. The failure of glass cylinders in diametral compression. J. Mech. Phys. Solids 19, 179–200.

ISRM (Co-ordinator: Ouchterlony, F.), 1988. Suggested methods for determining the fracture toughness of rock. Int. J. Rock Mech. Min. Sci. Geomech. Abstr. 25, pp. 71–96.

Jianhong, Y., Wu, F.Q., Sun, J.Z., 2009. Estimation of the tensile elastic modulus using Brazilian disc by applying diametrically opposed concentrated loads. Int. J. Rock Mech. Min. Sci. 46, 568–576.

Kourkoulis, S.K., Exadaktylos, G.E., Vardoulakis, I., 1999. *U*-notched Dionysos Pentelicon marble in three point bending: the effect of nonlinearity, anisotropy and microstructure. Int. J. Fract. 98, 369–392.

Kourkoulis, S.K., Markides, Ch.F., Chatzistergos, P.E., 2012. The contact length in the standardized Brazilian disc test: an analytic and experimental approach. Int. J. Solids Struct. accepted for publications.

Lavrov, A., Vervoort, A., 2002. Theoretical treatment of tangential loading effects on the Brazilian test stress distribution. Int. J. Rock Mech. Min. Sci. 39, 275–283.

Machida, A., 1975. Studies on tests for splitting tensile strength of concrete. Proc. Japanese Soc. Civil Eng. 242, 115–124.
Markides, Ch.F., Pazis, D.N., Kourkoulis, S.K., 2010. Closed full-field solutions for stresses and displacements in the Brazilian disk under distributed radial load. Int. J. Rock Mech. Min. Sci. 47, 227–237.
Markides, C.F., Pazis, D.N., Kourkoulis, S.K., 2011. Influence of friction on the stress field of the Brazilian tensile test. Rock Mech. Rock Eng. 44, 113–119.
Markides, Ch.F., Kourkoulis S.K., in press. The stress field in a standardized Brazilian disc: the influence of the loading type acting on the actual contact length. Rock Mech. Rock Eng. in press. doi:10.1007/s00603-11-0201-2.
Muskhelishvili, N.I., 1963. Some basic problems of the mathematical theory of elasticity, Groningen: Noordhoff, The Netherlands.
Sutton, M.A., McNeill, S.R., Helm, J.D., Chao, Y.J., 2000. Advances in two-dimensional and three-dimensional computer vision. In: Rastogi, P.K. (Ed.), Photomechanics, Topics Applied Physics, 77. Springer-Verlag, Berlin, Heidelberg, pp. 323–372.
Tong, J., Wong, K.Y., Lupton, C., 2007. Determination of interfacial fracture toughness of bone-cement interface using sandwich Brazilian disks. Eng. Fract. Mech. 74, 1904–1916.
Vardar, Ö., Finnie, I., 1975. An analysis of the Brazilian disc fracture test using the Weibull probabilistic treatment of brittle strength. Int. J. Fract. 11 (3), 495–508.
Wijk, G., 1978. Some new theoretical aspects of indirect measurements of the tensile strength of rocks. Int. J. Rock Mech. Min. Sci. Geomech. Abstr. 15, 149–160.